Effect of form of obstacle on speed of crowd evacuation

Ryosuke Yano*
Tokio, Marine and Nichido Risk Consulting Co. Ltd., 1-5-1 Otemachi, Chiyoda-ku, Tokyo, Japan

(Received 3 July 2017; revised manuscript received 16 January 2018; published 29 March 2018)

This paper investigates the effect of the form of an obstacle on the time that a crowd takes to evacuate a room, using a toy model. Pedestrians are modeled as active soft matter moving toward a point with intended velocities. An obstacle is placed in front of the exit, and it has one of four shapes: a cylindrical column, a triangular prism, a quadratic prism, or a diamond prism. Numerical results indicate that the evacuation-completion time depends on the shape of the obstacle. Obstacles with a circular cylinder (C.C.) shape yield the shortest evacuation-completion time in the proposed model.

DOI: 10.1103/PhysRevE.97.032319

I. INTRODUCTION

The study of collective motion [1,2] in biological systems has attracted physicists' and mathematicians' attention, because models of these phenomena require rich physical and mathematical insights. In particular, Vicsek's pioneering work on collective motion [3,4] implemented insights from physics in order to model a biological collective motion system. The clustering of agents' velocity-vector angles toward a local angle, averaged over those of agents with a distance less than a threshold, yields a characteristic spatial structure [3,5–10]. This convergence toward an averaged value over a finite range is also implemented in the Hegselmann-Krause model of opinion formation [11]. Similarly, several mathematical models such as the Cucker-Smale model [12], the self-propulsion–repulsive-attractive model with drag force [13,14], and the Kuramoto-Vicsek model [15,16] have been used in order to model biological swarming. Pedestrian collective motion has been studied by Helbing *et al.* [17,18], who used the social-force model [19] to investigate the key characteristics of pedestrian collective motion. Recently, Dietrich and Köster [20] proposed the gradient-navigation model for pedestrian collective motion. The attractive-repulsive force and acceleration or deceleration due to the relaxation of pedestrian velocities toward their intended velocities [21] are considered to be significant characteristics of pedestrian collective motion. Many discrete element method (DEM) simulations [22–25] have been performed which implemented Helbing and Molnar's social-force model [21], whereas cellular automata [26,27] have been also considered as an application of game theory in pedestrian dynamics.

Meanwhile, Helbing proposed a collective-motion model that uses a hydrodynamic equation derived from the Boltzmann equation [28–30]. This equation includes a distribution function with five dimensions, namely, $f(t,\boldsymbol{v},\boldsymbol{v}_{\rm in},\boldsymbol{x})$ ($t \in \mathbb{R}_+$: time; $\boldsymbol{x} \in \mathbb{R}^2$: physical space; $\boldsymbol{v} \in \mathbb{R}^2$: velocity space; $\boldsymbol{v}_{\rm in} \in \mathbb{R}^2$: intended velocity space). The derivation of hydrodynamic equations [31–34] such as the Navier-Stokes (NS) equation has been considered to model phase transitions in biological collective-motion systems. We consider, however, that collective phenomena of pedestrians are always beyond the Grad-Boltzmann or Grad-Enskog limit, because the number of pedestrians in a typical crowd is much smaller than the Avogadro number, as observed in the flow of granular materials [35]. Therefore, numerical modeling of pedestrian motion can offer insights beyond the hydrodynamic description derived from the Boltzmann-Enskog equation [22]. The network structure among destinations also has a significant effect on collective motion when movements of pedestrians occur among cities or countries [36], but this work focuses on a finer-grained level of analysis.

In this paper, we focus on how the shape of an obstacle affects the speed with which a crowd of pedestrians evacuates a room. Evacuation is an important application of collective-motion modeling [37] because excessive jamming in the flow of pedestrians can generate extremely hazardous, even fatal, conditions when a large crowd must quickly evacuate a room. The following discussion assumes that the forces between pedestrians can be modeled as spring-mass systems. Therefore, pedestrian dynamics are similar to those observed in active soft matter such as granular particles or soft disks [38] that have intended velocities. In order to realistically model pedestrian dynamics, the model must include representations of the following dynamic phenomena: herding (swarming) among neighboring pedestrians [39], the effect of visibility of vacant spaces or obstacles [39], route-choice strategies [40], avoiding injured or dead pedestrians as obstacles [41], the distribution of intended velocities in accordance with the age [42] or (competitive) character of pedestrians [43], the relationship between pedestrian density and intended velocity, the convergence rate toward the intended velocities [44], and the effect of polydisperse noncircular areas of personal space [45]. Obviously, these phenomena cannot all be represented with spring-mass interaction forces. A toy model with spring-mass forces, while not being totally realistic, can offer basic data about how the shape of an obstacle affects the evacuation-completion time. The spring constant in our model corresponds to the strength of an individual's repulsion from other pedestrians that infringe upon this individual's personal

*ryosuke.yano@tokiorisk.co.jp

space. Evacuation of pedestrians through a narrow exit has been modeled as a bottleneck flow of granular particles in the past [46–49], as the gravitational attraction of granular particles toward the bottleneck at the bottom of a hopper is analogous to a pedestrian's intended velocity. The relationships between the width of the exit and the evacuation-completion time and between the shape and location of an obstacle and the evacuation-completion time have been adequately studied in previous work [50,50,51]. Previous studies on the effects of obstacle shape, however, have only considered limited sets of possible shapes. Frank and Dorso [52] compared the effects of thin-plate and circular cylinder (C.C.) obstacles, and Stark *et al.* [53] compared the effects of triangular prisms (T.P.) with different vertex angles. Therefore, we modeled the effect of a wide range of obstacle shapes placed in front of an exit on the evacuation time. We modeled the above-mentioned C.C. and T.P. obstacle shapes, along with quadrangular prism (Q.P.) and diamond prism (D.P.) obstacles. The footprints of the four types of obstacles are equal in the models. We also modeled a large-scale evacuation of 2400 pedestrians from one room to another through an exit. The width of the exit allows ten pedestrians to pass through it at once without encroaching upon each other's personal space. Such an evacuation might occur in a large room, such as conference floor or an amphitheater. The numerical results from these simulations indicate that the evacuation-completion time is significantly affected by the shape of the obstacle. C.C. obstacles yield the shortest evacuation-completion time in our numerical simulations. If an exit in a room is unavoidably obstructed by a structural element, our results suggest that the obstacle should have a cylindrical shape in order to encourage efficient and safe evacuations. We also investigated the effect of the spring constant on the evacuation-completion time. The results suggest that the freezing-by-heating discovered by Helbing *et al.* [54] may correspond to an increase in the spring constant, if the volatility of Brownian pedestrian motion [55,56], namely, active Brownian particles, is fixed. Stanley [57] predicted that this freezing-by-heating discovered by Helbing *et al.* [54] might play an important role in crowd evacuations. Our model, however, cannot represent the melting transition by further heating via an increase in the spring constant, because the volatility of fluctuations [56] is fixed in the model. This paper seeks an understanding of how pedestrians evacuate buildings by visualizing the force-chain network [58] together with the flow velocity as calculated by spatially coarse-graining pedestrian velocities.

II. NUMERICAL METHOD TO CALCULATE EVACUATION

The dynamics of pedestrian motion are modeled as simple interactions by regarding pedestrians as active soft matter, namely, granular disks with intended velocities. The conventional numerical method, which has been used to calculate the dynamics of granular matter, is also applied to the simulation of the evacuation of pedestrians, exclusively.

A schematic of the pedestrian dynamics is shown in Fig. 1. A soft two-dimensional disk of radius R models the effect of one pedestrian occupying a domain. R is not the domain occupied by the real physical volume of the pedestrian, but instead it represents a social domain, because two pedestrians will feel

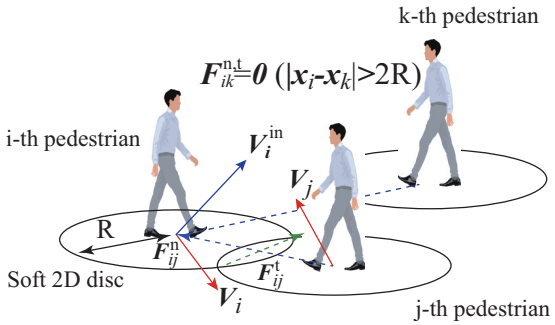

FIG. 1. Schematic of dynamics of pedestrian (R: radius of circular private domain; x_i: location of pedestrian indexed by i; $\boldsymbol{v}_i$: velocity of pedestrian indexed by i; $\boldsymbol{v}_i^{\text{in}}$: intended velocity of pedestrian indexed by i; $\boldsymbol{F}_{ij}^n$ and $\boldsymbol{F}_{ij}^t$: normal and tangential forces between two interacting pedestrians indexed by i and j).

stress (forces) when their personal spaces overlap. If we were to model the actual diverse sizes of pedestrians, polydisperse disks with different radii R [59] would need be considered. We leave the consideration of polydisperse disk sizes for future work, for the sake of simplicity in this study.

A repulsive force [60] appears when the distance between two pedestrians is less than $2R$; normal and tangential force components are considered. The tangential component, which presents realistic cohesion [61] between two interacting pedestrians, is beyond the scope of this paper. We neglect the torque on the active particles caused by the tangential component of the interaction in order to simplify the following discussion. Finally, the set of parameters used in our numerical model should be determined from the experimental results [62,63] of pedestrian motion. The development of big-data technology allowed us to observe pedestrian motion using Wi-Fi [64] and video data.

The normal force ($\boldsymbol{F}_{ij}^n$) and tangential force ($\boldsymbol{F}_{ij}^t$) between two interacting pedestrians indexed by i and j are calculated as follows (the subscript in $\boldsymbol{F}_{ij}^{n,t}$ indicates forces received by the ith pedestrian from the jth pedestrian):

$$\begin{aligned}
\boldsymbol{F}_{ij}^n &= -k_{pp}(|\boldsymbol{x}_i - \boldsymbol{x}_j| - 2R)\boldsymbol{e}_{ij}^n,\\
\boldsymbol{F}_{ij}^t &= \mu_{pp}F_{ij}^n\boldsymbol{e}_{ij}^t\\
\boldsymbol{e}_{ij}^n &= \frac{\boldsymbol{x}_i - \boldsymbol{x}_j}{|\boldsymbol{x}_i - \boldsymbol{x}_j|},\\
\boldsymbol{e}_{ij}^t &= -\text{sgn}\left[\varphi(-\pi/2)\boldsymbol{e}_{ij}^n \cdot (\boldsymbol{g}_{ij}/|\boldsymbol{g}_{ij}|)\right]\varphi(-\pi/2)\boldsymbol{e}_{ij}^n, \quad (1)
\end{aligned}$$

where $\boldsymbol{x}_i$ is the coordinate of the center of the disk, $k_{pp} \in \mathbb{R}_+$ is the spring constant, μ_{pp} is the friction coefficient if F_{ij}^t follows Coulomb friction, $\varphi(\theta)$ is a 2×2 rotation matrix by θ, and $\boldsymbol{g}_{ij} := \boldsymbol{v}_i - \boldsymbol{v}_j$ is the relative velocity between two interacting pedestrians indexed by i and j. In the social-force model by Helbing and Vicsek [21], the social force, which obeys the exponential function of the distance between two pedestrians, is added to $\boldsymbol{F}_{ij}^n$, in order to inhibit the ith pedestrian from passing through the jth pedestrian, whereas we neglect such a social force, which obeys an exponential function of the distance between two pedestrians, in order to focus on the effect of the spring constant on the evacuation-completion time.

Next, the inelastic collisions between two inelastic disks are expressed with the damper equipped with the spring. Additionally, we consider fluctuations in pedestrian motion as a Brownian motion. Fluctuations in pedestrian motion might be caused by attempts to avoid collisions or the impatience in choosing walking trajectories. Therefore, we conjecture that an increase in the volatility of motion fluctuations slows down the evacuation speed, because deviations from the intended velocity lengthen the total path that each pedestrian takes to an exit. On the other hand, we also conjecture that clogging of pedestrians around an exit is alleviated, as observed in the transition from jamming to unjamming, when a silo is vibrated [65]. Thus, fluctuations may have significant effects on pedestrian collective motion, as observed in freezing-by-heating by Helbing *et al.* [28]. The time evolution of the velocity of the ith pedestrian, accounting for collisions between pairs of pedestrians and fluctuations [66], is formulated as

$$\frac{d\boldsymbol{v}_i}{dt} = \sum_{j\neq i} \Theta(2R - |\boldsymbol{x}_i - \boldsymbol{x}_j|)\left(\boldsymbol{F}^n_{ij} + \boldsymbol{F}^t_{ij}\right) - D|\boldsymbol{v}_i|^\beta \left(\frac{\boldsymbol{v}_i}{|\boldsymbol{v}_i|}\right) + \xi d_t B_i, \tag{2}$$

where $D \in (\mathbb{R}_+ \cup 0)$ is the damping rate, $\beta \in \mathbb{R}_+$, $\mathrm{sgn}(x)$ is the signature of x, $\Theta(2R - |\boldsymbol{x}_i - \boldsymbol{x}_j|)$ is Heaviside's step function, B_i ($\xi \in \mathbb{R}_+$) is the Wiener process, and the mass of each circle is set to unity for the sake of simplicity. Our choice to describe fluctuations with the Wiener process must be validated in future work, as pedestrian motion is sometimes described by a Lévy walk [67]. $D = 0$ in Eq. (2) corresponds to the perfectly elastic collisions between pairs of interacting pedestrians. In Helbing's social-force model [28], the attractive force, which sometimes forms pedestrian groups with a characteristic velocity [68], is considered together with the repulsive force. We neglect such an attractive force, because we consider that attractive forces among pedestrians are not appropriate for describing an evacuation scenario, in which all the pedestrians try to reach the exit at a relative high intended velocity. Evacuation scenarios seem to encourage competitive motion, which decreases the swarming behavior that the attractive force is meant to represent.

Finally, the velocities of pedestrians converge to their intended velocities ($\boldsymbol{v}_i^{\mathrm{in}}$), and directions turn toward the exit. Adding the relaxation of the velocities of pedestrians toward their intended velocities, Eq. (2) is modified as

$$\frac{d\boldsymbol{v}_i}{dt} = \sum_{j\neq i} \Theta(2R - |\boldsymbol{x}_i - \boldsymbol{x}_j|)\left(\boldsymbol{F}^n_{ij} + \boldsymbol{F}^t_{ij}\right) - D|\boldsymbol{v}_i|^\beta \frac{\boldsymbol{v}_i}{|\boldsymbol{v}_i|} + \xi d_t B_i + \zeta\left(\boldsymbol{v}_i^{\mathrm{in}} - \boldsymbol{v}_i\right), \tag{3}$$

where $\zeta \in \mathbb{R}_+$ is the rate at which the velocities converge to the "constant" intended velocity. Of course, ζ of pedestrians who can see an exit will be larger than that of pedestrians who cannot see the exit, whereas a constant ζ is used in this study. Provided that ζ is large such that effects of fluctuations may be neglected, all the pedestrians move toward the exit at their intended velocities. On the other hand, if ξ is large enough such that the convergence of the velocity may be neglected, pedestrians tend to move toward isotropic directions. The effects of variations in the intended velocities are interesting, as observed in agents who ignore the traffic rules in traffic flow [69] or in the variation of their intended velocities in accordance with age [42]. Theses effects are, however, beyond the scope of this study.

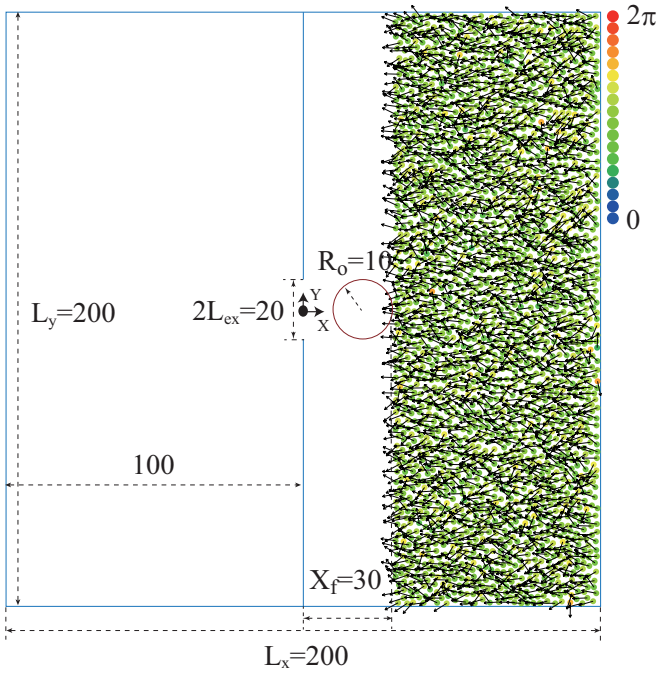

FIG. 2. Schematic of evacuation of 2400 pedestrians at $t = 0$, when the shape of the obstacle is C.C. The color of a circle corresponds to the angle of initial velocity $\theta_i \in [0, 2\pi)$ of a pedestrian indexed by i in Eq. (4).

The interaction between a pedestrian and an obstacle or wall is modeled in a way similar to how interpedestrian interactions are modeled with Eq. (1). The spring constant (k) that determines force between a pedestrian and obstacle is k_{po}, and spring constant between the pedestrian and wall is k_{pw}, where friction coefficients in the interaction between the pedestrian-obstacle and wall are defined by μ_{po} and μ_{pw}, respectively. During an interaction with an obstacle or a wall, the pedestrian velocities never relax to their intended velocities and are never damped.

III. PARAMETERS USED IN NUMERICAL STUDY

We investigate the evacuation of pedestrians through an exit from the right room to the left room, which are partitioned by the wall. A schematic of the numerical domain is shown in Fig. 2, when the shape of the obstacle is C.C. In the discussion below, all the physical quantities are normalized. A square domain ($\mathbb{X} \subseteq \mathbb{R}^2$) stretched by $X, Y \in \mathbb{X} | X \in [-L_x/2, L_x/2] \wedge Y \in [-L_y/2, L_y/2]$ is considered, in which $L_x = L_y = 2L = 200$. The walls are set along the lines $X = -L_x/2, Y \in [-L, L]$, $X = L, Y \in [-L, L]$, $X \in [-L, L], Y = -L$, $X \in [-L, L], Y = L$, $X = 0, Y \in [Y_{\mathrm{ex}}, L]$, and $X = 0, Y \in [-L, -Y_{\mathrm{ex}}]$, as shown in Fig. 2. The exit is placed at $X = 0$, $Y \in (-L_{\mathrm{ex}}, L_{\mathrm{ex}})$, in which $L_{\mathrm{ex}} = 10$. $N_{\mathrm{tot}} = 2400$ pedestrians are placed randomly in the domain $(X, Y) \in \mathfrak{X}_0 | X \in (X_f + R, L - R], Y \in [-L + R, L - R]$, where R is

set to unity and $X_f = 30$. The directions of initial velocities of pedestrians are sampled using the Maxwell-Boltzmann distribution, whose temperature is equal to 0.5 and mean value is π; in short,

$$\theta_i = \bar{\theta} + \sqrt{-\theta_\infty \ln a}\cos(2\pi b), \quad \bar{\theta} = \pi,\ \theta_\infty = 5,$$
$$a \in (0,1],\ b \in (0,1], \tag{4}$$

where a and b are white noise terms and $\theta \in (0,2\pi]$. Of course, these initial conditions are idealized for our numerical study. The absolute values of pedestrian velocities ($|\boldsymbol{v}|$) are fixed to unity at $t = 0$. Consequently, $(v_x^i, v_y^i) = (\cos\theta_i, \sin\theta_i)$ at $t = 0$.

The initial domain occupied by pedestrians at $t = 0$ is fixed to $\mathfrak{X}_0$ regardless of shape of the obstacle. Additionally, the area occupied by the obstacle in $\mathbb{X}$ is fixed to a constant value and its right edge, namely, the maximum value of X in the domain of the obstacle, is fixed to $X = X_f = 30$. The center of the C.C. obstacle is set at $(X_c, Y_c) = (20,0)$ and its radius is set to $R_c = 10$. Here, $\boldsymbol{x} \in \mathfrak{X}_p^i || \boldsymbol{x} - \boldsymbol{x}_i| \leqslant R$ represents the domain occupied by the ith pedestrian and $\boldsymbol{x} \in \mathfrak{X}_o$ represents the domain occupied by the obstacle. As a result, the area of the obstacle in $\mathbb{X}$ is fixed to πR_c^2. We consider four types of shapes of the obstacle, namely, C.C, Q.P., T.P., and D.P. The length of one side of the square in the case of the Q.P. is set to $\sqrt{\pi} R_c$ and length of the side of the triangle vertical to the X axis is set to $2\sqrt{3\sqrt{3}\pi}\, R_c$, when the vertex of the isosceles triangle is set to $\pi/3$.

$k_{pw} = 10^3$, $k_{po} = 10^4$, $\mu_{pp} = \mu_{pw} = 0.1$, $\mu_{po} = \mu_{pp} k_{pp}/k_{po}$, $D = 1$, $\beta = 1$, $\xi = 1$, and $\zeta = 10$ are used in Eqs. (1)–(3).

The intended velocities of pedestrians are modeled as follows:

$$\boldsymbol{v}_i^{\text{in}} = (-1,0) \quad \text{in } x_i \in [R, L-R) \wedge y_i \in (-L_{\text{ex}} + R, L - R) \wedge \mathfrak{X}_p^i \cap \mathfrak{X}_o = \emptyset,$$
$$\boldsymbol{v}_i^{\text{in}} = (\cos\theta_3, \sin\theta_3) \quad \text{in } x_i \in [0, L-R) \wedge y_i \in (-L + R, -L_{\text{ex}} + R] \wedge \mathfrak{X}_p^i \cap \mathfrak{X}_o = \emptyset,$$

where

$$\theta_1 = \pi - \tan^{-1}\left(\frac{-L_{\text{ex}} + R - y_i}{x_i}\right),$$
$$\theta_2 = \pi - \tan^{-1}\left(\frac{L_{\text{ex}} - R - y_i}{x_i}\right),$$
$$\theta_3 = \theta_2 + (\theta_1 - \theta_2)\mathscr{W}_1;$$

$$\boldsymbol{v}_i^{\text{in}} = (\cos\theta_6, \sin\theta_6) \quad \text{in } x_i \in [R, L-R) \wedge y_i \in [L_{\text{ex}} - R, L - R) \wedge \mathfrak{X}_p^i \cap \mathfrak{X}_o = \emptyset,$$

where

$$\theta_4 = \pi + \tan^{-1}\left(\frac{y_i - (L_{\text{ex}} - R)}{x_i}\right),$$
$$\theta_5 = \pi + \tan^{-1}\left(\frac{y_i - (-L_{\text{ex}} + R)}{x_i}\right),$$
$$\theta_6 = \theta_4 + (\theta_5 - \theta_4)\mathscr{W}_2;$$

$$\boldsymbol{v}_i^{\text{in}} = (0,0) \quad \text{in } x_i \in [-L, R] \wedge y_i \in (-L, L) \wedge \mathfrak{X}_p^i \cap \mathfrak{X}_o = \emptyset,$$

where $\mathscr{W}_1, \mathscr{W}_2 \in [0,1]$ are white noise terms. The above model does not include pedestrians' route choices [70], such as choices to move toward more vacant space or to avoid collisions [71]. In previous studies [21,72], $\zeta = 2\text{s}^{-1}$, $|\boldsymbol{v}^{\text{in}}| = 1.34\,\text{m s}^{-1}$, the contact distance $R \sim 0.5 \pm 0.2$ m, and $k_{pp} \sim 2000$ N (when the repulsive force is defined as an exponential function of the distance between two pedestrians [72]). Therefore, the set of parameters in the present simulation is similar to that used in previous studies [21,72], if nondimensionalized physical quantities $L_\infty = 1.0$ m and $t_\infty = 1$ s are assumed, although $\zeta = 10\ \text{s}^{-1}$ is larger than $\zeta = 2\ \text{s}^{-1}$, because we postulate an evacuation. ξ, β, D, μ_{pi} $(i = p,w,o)$, and k_{pi} $(i = w,o)$ are, however, fixed artificially, because their concrete values are not determined for evacuation scenarios. For example, $\xi = |\boldsymbol{v}^{\text{in}}| = 1$ might be plausible, when the units of these quantities are m s^{-1}. A more realistic set of parameters must be obtained using data of real evacuations or evacuation drills.

The normalized time interval is set to 2.5×10^{-3} and the contour of the circle in Fig. 2 corresponds to the angle of $\boldsymbol{v}_i$. In the present numerical study, evacuations of 2400 pedestrians from the right room to the left room are simulated, as shown in Fig. 2. Therefore, the modeled evacuations occur in a large space (i.e., two rooms of 2×10^4 m^2), which usually has multiple emergency exits [73,74]. We, however, consider only one exit in order to isolate the effect of the shape of the obstacle on the evacuation-completion time.

IV. NUMERICAL RESULTS

Following the numerical method discussed in Sec. II, evacuations of 2400 pedestrians are simulated using the obstacle whose shape is C.C., Q.P., T.P., or D.P. Figure 3 shows snapshots of pedestrians at $t = 120$ and 300 moving around C.C., Q.P., T.P., and D.P obstacles, when $k_{pp} = 100$ or 10^3. The color of the circles corresponds to the vector angle of the pedestrians' velocities, namely, $\theta_i := \tan^{-1}(v_i^y/v_i^x)$ (i: index of agent). Figures 3 shows that the area occupied by pedestrians decreases as k_{pp} decreases. This trend reflects the fact that the repulsion force from the modeled spring when $r_{ij} < R$ tends to inhibit the invasion of other pedestrians indexed by j inside the private domain ($\boldsymbol{x}_i \in \mathfrak{X}_p^i$) via the increase in k_{pp}. As a result, the volatility of θ_i in the calculation domain increases as k_{pp} increases, in particular, in front of the obstacle ($X > X_f$), for any shape of obstacle, as shown in Fig. 3. In short, the standard deviation of thermal fluctuations in pedestrian motion increases in accordance with the spring constant. Such thermal fluctuations were interpreted as kinetic stress (or in other words, static pressure in the gas dynamics) by Garcimartin *et al.* [75]. They indicated that kinetic stress has more significant effects on the overall evacuation pattern than the local density does. Additionally, Fig. 3 shows that the spatial distributions of pedestrians are almost symmetric in cases of C.C, Q.P., and T.P, whereas the distributions of

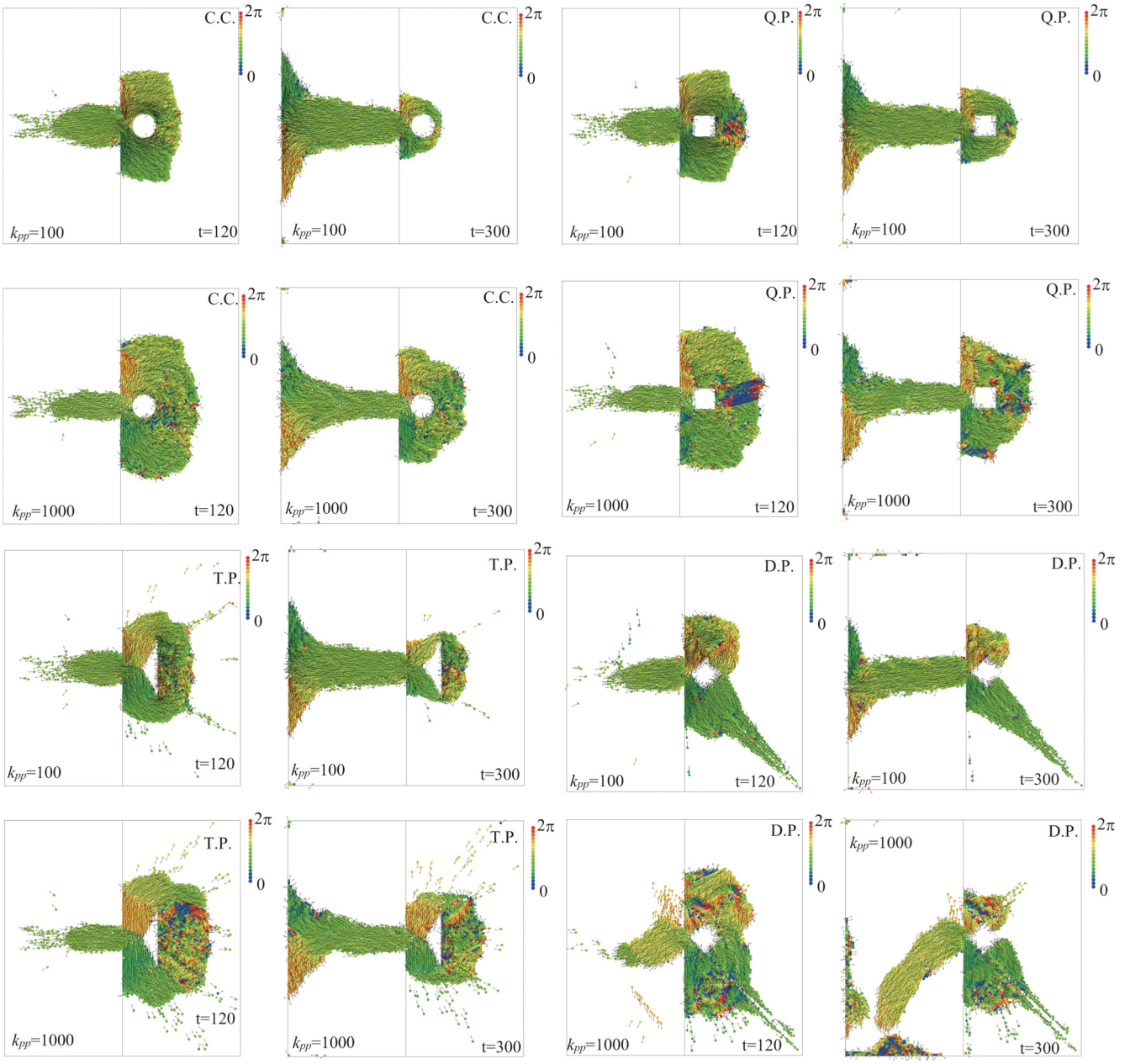

FIG. 3. Snapshots of pedestrians at $t = 120$ (left-half frames) and 300 (right-half frames) in cases of C.C. Q.P., T.P., and D.P., when $k_{pp} = 100$ and 10^3 (k_{pp}: spring constant). The color of a circle corresponds to the angle of velocity $\theta_i \in [0, 2\pi)$ of a pedestrian indexed by i.

pedestrians are asymmetric in the case of D.P. We found characteristic distributions of pedestrians along $Y = -X, X > X_f$ in the case of D.P., as shown in Fig. 3. The answer to the reason why such a characteristic distribution is obtained in the case of D.P. is left as a topic for future research, where the investigation of the bifurcation [76] of both density of pedestrians and its temporal variation at an exit in accordance with the rotation angle of Q.P. around its center axis might be of interest.

Figure 4 shows streamlines at $t = 120$ and 300 in cases of C.C., Q.P., T.P., and D.P, when $k_{pp} = 10^3$. The flow velocity is calculated by averaging the velocities of the pedestrians included inside each cell, which is formed by 30×30 equally spaced grids in $\mathbb{X}$. Figure 4 shows that no vortex occurs at $t = 120$ in the case of C.C., whereas many vortices occur at $t = 120$ in the case of T.P. Marked vortices are not generated in the case of D.P., when compared with T.P. and Q.P. An analysis of the turbulence of the flowfield [77–79] in cases of C.C. at $t = 300$, T.P., and Q.P. is noted as a topic for future research.

Next, we consider the force-chain network in the case of C.C., when $k_{pp} = 10$, 100, or 10^3. Figure 5 shows the force-chain network obtained using $k_{pp} = 10$ (top frame), 100 (middle frame) and 10^3 (bottom frame). Figure 5 shows that the number of links connected to a node (or pedestrian) increases as k_{pp} decreases. The length of a link corresponds to the distance between two interacting pedestrians. Thus, the density can be calculated in terms of the length of the links. On the other hand, the lengths of all the links are equal to R in the case of

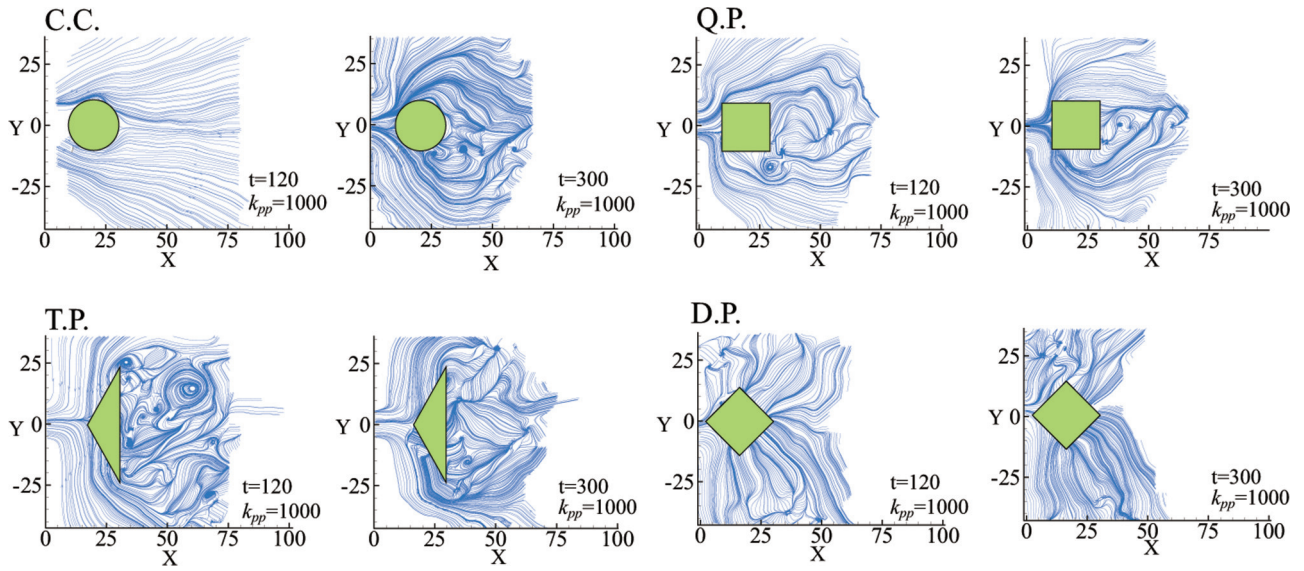

FIG. 4. Streamlines of flow velocity at $t = 120$ and 300 in cases of C.C., Q.P., T.P., and D.P., when $k_{pp} = 10^3$ (k_{pp}: spring constant).

$k_{pp} = 10^3$. Therefore, no marked compression of the personal domain $\mathfrak{X}_p^i$ occurs in the case of $k_{pp} = 10^3$. Consequently, the local number density never surpasses the maximum value obtained by calculating the closest packing of disks in the case of $k_{pp} = 10^3$. Figure 5 indicates that a shock layer forms in the cases of $k_{pp} = 10$ and 100. A schematic of this phenomenon is shown in Fig. 6. The shock-detachment distance (ℓ_s) increases as k_{pp} increases, whereas a dilute region forms behind C.C. owing to the expansion wave. Another interesting result is that low-density lanes form in the case of $k_{pp} = 10^3$. The reader may readily confirm that the nontriangular lattices form lanes in the range of $X > 0$, as shown in the bottom frame of Fig. 5.

Figure 7 plots the number of links (l) versus its distribution function, $f(l) := 1/N_{\rm tot} \sum_{i=1}^{N_{\rm tot}} \delta(l - l_i)$ (l_i: number of links connected to pedestrian indexed by i) at $t = 120$ obtained using $k_{pp} = 10$, 100, and 10^3 in the case of C.C. $f(l) \in \mathbb{R}_+$ is obtained in the range of $l \in [0,28] \cap \mathbb{Z}_+$ in the case of $k_{pp} = 10$, $f(l) \in \mathbb{R}_+$ is obtained in the range of $l \in [0,10]$ in the case of $k_{pp} = 100$, and $f(l) \in \mathbb{R}_+$ is obtained in the range of $l \in [0,6]$ in the case of $k_{pp} = 10$. Therefore, the number of links increases as k_{pp} decreases. The maximum of $f(l)$ is obtained at $l = 6$, which corresponds to the closest packing of hard disks, in the case of $k_{pp} = 10^3$, whereas the maximum of

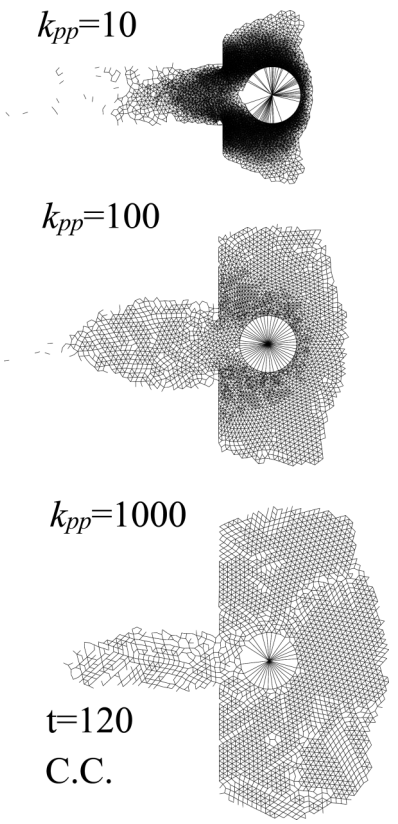

FIG. 5. Snapshots of the force chain network at $t = 120$ in the case of C.C., when $k_{pp} = 10$ (top frame), 100 (middle frame), and 10^3 (bottom frame) (k_{pp}: spring constant).

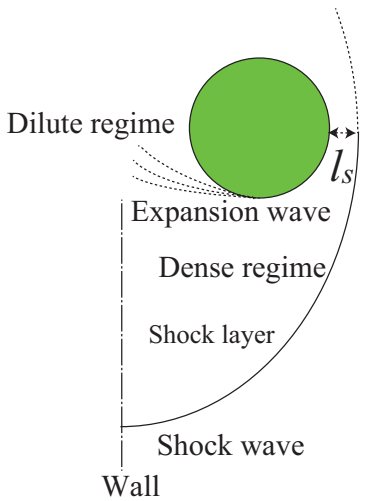

FIG. 6. Schematic of the flow field in the case of C.C. (l_s: shock-detachment distance).

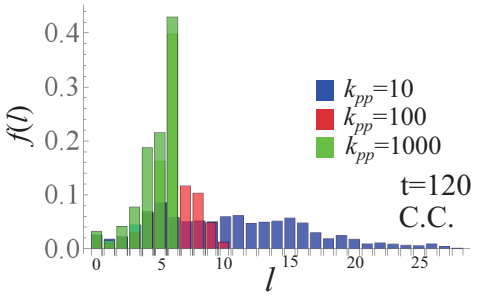

FIG. 7. l (number of links) versus $f(l)$ (distribution function of link number) obtained using $k_{pp} = 10$, 100, and 10^3 (k_{pp}: spring constant) at $t = 120$ in the case of C.C.

$f(l)$ is obtained at $l = 7$ in the case of $k_{pp} = 100$ and obtained at $l = 4$ in the case of $k_{pp} = 10$. $f(l)$ obtained using $k_{pp} = 10$ seems to be a plateau in the range of $l \in [6,11]$, whereas $f(l)$ obtained using $k_{pp} = 10^3$ increases in the range of $l \in [1,6]$, and $f(l)$ obtained using $k_{pp} = 100$ is bimodal, with peaks at $l = 5$ and 7.

Finally, we investigate the relationship between the evacuation-completion time and shape of the obstacle. First, the effect of the spring constant (k_{pp}) on the evacuation-completion time is investigated. Figure 8 plots the number of pedestrians evacuated ($N_{\rm ev} = |\cup_{i,x_i<0} i|$) versus elapsed time ($t$), which is measured from the start time of evacuation ($t = 0$) in cases of C.C. (upper-left frame), Q.P. (upper-right frame), T.P. (lower-left frame), and D.P. (lower-right frame). Three values of k_{pp}, namely, 100, 500, and 10^3, are used in cases of Q.P., T.P., and D.P., whereas another value of k_{pp}, namely 10, is added in the case of C.C. The evacuation-completion time ($t_{\rm ev} := \min_t \forall x_i(t) < 0$) decreases as k_{pp} increases in the case of C.C., whereas $t_{\rm ev}$ obtained using $k_{pp} = 500$ is quite similar to that obtained using $k_{pp} = 10^3$. The evacuation rate ($d_t N_{\rm ev}$) increases in $[0,t_1]$ ($d_t^2 N_{\rm ev}|_{t=t_1} = 0$) and decreases in $t \in [t_1,t_{\rm ev}]$ when $k_{pp} = 10$ and 100, whereas $d_t N_{\rm ev}$ is a positive constant in most of the range of $t \in [0,t_{\rm ev}]$ when $k_{pp} = 500$ and 10^3, in

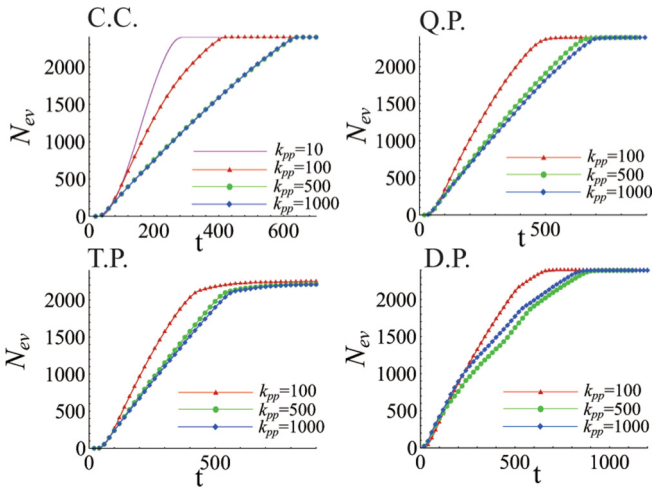

FIG. 8. t versus N_{ev} (number of pedestrians who finished their evacuations) in cases of C.C (upper-left frame), Q.P. (upper-right frame), T.P. (lower-left frame), and D.P. (lower-right frame).

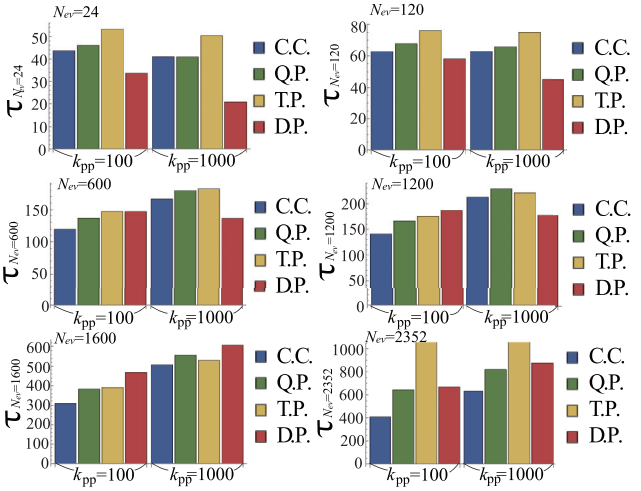

FIG. 9. $\tau_{N_{\rm ev}}$ (elapsed time required by evacuations of $N_{\rm ev}$ pedestrians) obtained using $k_{pp} = 100$ and $k_{pp} = 10^3$ (k_{pp}: spring constant) in cases of C.C., Q.P., T.P., and D.P., when $N_{\rm ev} = 24$, 120, 600, 1200, 1600, and 2352.

cases of C.C, Q.P., and T.P. $t_{\rm ev}$ decreases as k_{pp} increases in the case of C.C., whereas $t_{\rm ev}$ obtained using $k_{pp} = 500$ is quite similar to that obtained using $k_{pp} = 10^3$. Consequently, we can understand that freezing-by-heating is obtained by increasing k_{pp}, because the increase in k_{pp} yields a decrease in loss of kinetic energy of the pedestrian via inelastic collisions with other pedestrians, and we can regard the increase in k_{pp} as the heating. On the other hand, we must confirm whether the further increase in k_{pp} changes $t_{\rm ev}$ by changing the solid state to the gaseous state in our future study. At least, the phase of flow field obtained using $k_{pp} = 10$ and 100 seems to be liquid phase, as shown in Fig. 5. The increase in $t_{\rm ev}$ in accordance with the increase in k_{pp} is also obtained in cases of Q.P and T.P., whereas $t_{\rm ev}|_{k_{pp}=100} < t_{\rm ev}|_{k_{pp}=10^3} < t_{\rm ev}|_{k_{pp}=500}$ is obtained in the case of D.P. Such a characteristic behavior in the case of D.P. is probably caused by the characteristic distribution of pedestrians in the case of D.P., as shown in Fig. 3. $N_{\rm ev}|_{k_{pp}=100}$ is similar to $N_{\rm ev}|_{k_{pp}=500,10^3}$ in $t \in [0,200]$ in the case of D.P, whereas the nonlinear behavior of $N_{\rm ev}|_{k_{pp}=500,10^3}$ is marked in $t \in [200,t_{\rm ev}]$. As with the case of T.P., the complete evacuation of pedestrians from the right room to the left room is not obtained, because some pedestrians remain to the right of T.P., namely, $x_i > X_f$. The increase in the volatility of fluctuations might enable the complete evacuation in the case of T.P.

Finally, we investigate effects of the shape of the obstacle on $\tau_{N_{\rm ev}}$, which is the time required by evacuations of $N_{\rm ev}$ pedestrians. In cases of both $k_{pp} = 100$ and 10^3, $t_{\rm ev}|_{\rm C.C.} < t_{\rm ev}|_{\rm Q.P.} < t_{\rm ev}|_{\rm D.P.} < t_{\rm ev}|_{\rm T.P.}$ is obtained, as shown in Fig. 8. Figure 9 shows $\tau_{N_{\rm ev}}$ obtained using $k_{pp} = 100$ and 10^3 in cases of C.C., T.P., Q.P., and D.P., when $N_{\rm ev} = 24$ (1% of total pedestrians), 120 (5% of total pedestrians), 600 (25% of total pedestrians), 1200 (50% of total pedestrians), 1600 (67% of total pedestrians), and 2,352 (98% of total pedestrians). $\tau_{N_{\rm ev}}$ obtained using $k_{pp} = 100$ in the case of D.P. is smaller than $\tau_{N_{\rm ev}}$ obtained using $k_{pp} = 100$ in cases of C.C. T.P., and Q.P., when $N_{\rm ev} \leqslant 600$. Similarly, $\tau_{N_{\rm ev}}$ obtained using $k_{pp} = 10^3$ in the case of D.P. is smaller than $\tau_{N_{\rm ev}}$ obtained using $k_{pp} = 10^3$

in cases of C.C., T.P., and Q.P., when $N_{\rm ev} = 24$, 120, 600, and 1200. We can confirm that the most rapid evacuation is obtained using the D.P. in the early stage of the evacuation. In short, $\tau_{N_{\rm ev}}|_{\rm D.P.} < \tau_{N_{\rm ev}}|_{\rm C.C.} < \tau_{N_{\rm ev}}|_{\rm Q.P.} < \tau_{N_{\rm ev}}|_{\rm T.P.}$ is obtained using $k_{pp} = 100$, when $\tau_{N_{\rm ev}} \leqslant 600$. Meanwhile, $\tau_{N_{\rm ev}}|_{\rm C.C.} < \tau_{N_{\rm ev}}|_{\rm Q.P.} < \tau_{N_{\rm ev}}|_{\rm T.P.} < \tau_{N_{\rm ev}}|_{\rm D.P.}$ is obtained using $k_{pp} = 100$, when $\tau_{N_{\rm ev}} = 1200$ and 1600. Finally, $\tau_{N_{\rm ev}}|_{\rm C.C.} < \tau_{N_{\rm ev}}|_{\rm Q.P.} < \tau_{N_{\rm ev}}|_{\rm D.P.} < \tau_{N_{\rm ev}}|_{\rm T.P.}$ is obtained using $k_{pp} = 100$, when $\tau_{N_{\rm ev}} = 2{,}352$, because there exist pedestrians who cannot evacuate from the right room to the left room, as shown in Fig. 8 in the case of T.P. $\tau_{N_{\rm ev}}|_{\rm D.P.} < \tau_{N_{\rm ev}}|_{\rm C.C.} < \tau_{N_{\rm ev}}|_{\rm Q.P.} < \tau_{N_{\rm ev}}|_{\rm T.P.}$ is obtained using $k_{pp} = 10^3$, when $\tau_{N_{\rm ev}} = 24$, 120, and 600. $\tau_{N_{\rm ev}}|_{\rm D.P.} < \tau_{N_{\rm ev}}|_{\rm C.C.} < \tau_{N_{\rm ev}}|_{\rm T.P.} < \tau_{N_{\rm ev}}|_{\rm Q.P.}$ is obtained using $k_{pp} = 10^3$, when $\tau_{N_{\rm ev}} = 1200$, whereas $\tau_{N_{\rm ev}}|_{\rm C.C.} < \tau_{N_{\rm ev}}|_{\rm T.P.} < \tau_{N_{\rm ev}}|_{\rm Q.P.} < \tau_{N_{\rm ev}}|_{\rm D.P.}$ is obtained using $k_{pp} = 10^3$, when $\tau_{N_{\rm ev}} = 1{,}600$. Finally, $\tau_{N_{\rm ev}}|_{\rm C.C.} < \tau_{N_{\rm ev}}|_{\rm Q.P.} < \tau_{N_{\rm ev}}|_{\rm D.P.} < \tau_{N_{\rm ev}}|_{\rm T.P.}$ is obtained using $k_{pp} = 10^3$, when $\tau_{N_{\rm ev}} = 2352$. In future work, we plan to examine whether the decrease in $N_{\rm ev}$ from 2400 would indicate which $t_{\rm ev}|_{\rm D.P.}$ is the smallest among four types of obstacles. As far as our numerical study shows, C.C. is, however, the best choice in order to realize the shortest evacuation-completion time, when an obstacle with a constant area must be placed in front of an exit.

V. CONCLUDING REMARKS

In this paper, we investigated effects of the shape of the obstacle on the evacuation-completion time using four types of the shape, namely, C.C., Q.P., T.P., and D.P. The evacuation of 2400 pedestrians was calculated using the DEM. A toy model, which regards the pedestrians as active soft matter based on the spring-mass system, was considered as the initial study of effects of the shape of the obstacle on the evacuation-completion time. The number of links in the force-chain network increases as the spring constant decreases. The closest packing is obtained when the spring constant (k_{pp}), which determines the interaction between pairs of pedestrians, is equal to 10^3. The length of links in the force-chain network indicates that a shock layer is formed around C.C. Additionally, many vortices are generated forward of the obstacle in the case of T.P. The increase in k_{pp}, namely, decrease in inelasticity, yields an increase in the evacuation-completion time in cases of C.C., Q.P., and T.P., whereas such a tendency does not always hold true for D.P. The evacuation-completion time obtained using C.C. is shortest among the four types of the shape of the obstacle. Meanwhile, the shortest evacuation-completion time is obtained by D.P., when the elapsed time is short.

[1] A. Czirók and T. Vicsek, Statistical mechanics of biocomplexity, in *Proceedings of the XV Sitges Conference, Barcelona, 1998*, edited by D. Reguera, J. M. G. Vilar, and J. M. Rubi (Springer, Berlin, 2010), pp. 152–164.
[2] A. Czirók, Phys. Rev. E **54**, 1791 (1996).
[3] T. Vicsek, A. Czirók, E. Ben-Jacob, I. Cohen, and O. Shochet, Phys. Rev. Lett. **75**, 1226 (1995).
[4] T. Vicsek and A. Zafeiris, Phys. Rep. **517**, 71 (2012).
[5] A. Czirók and T. Vicsek, Physica A **281**, 17 (2000).
[6] A. Czirók, H. E. Stanley, and T. Vicsek, J. Phys. A **30**, 1375 (1997).
[7] M. Durve and A. Sayeed, Phys. Rev. E **93**, 052115 (2016).
[8] F. Peruani, A. Deutsch, and M. Bar, Eur. Phys. J. Spec. Top. **157**, 111 (2008).
[9] K.-D. Nguyen, New J. Phys. **17**, 113056 (2015).
[10] M. Aldana, V. Dossetti, C. Huepe, V. M. Kenkre, and H. Larralde, Phys. Rev. Lett. **98**, 095702 (2007).
[11] R. Hegselmann and U. Krause J. Artif. Soc. Social Simul. **5**, 2 (2002).
[12] F. Cucker, and S. Smale, Jpn. J. Math. **2**, 197 (2007).
[13] M. R. D'Orsogna, Y. L. Chuang, A. L. Bertozzi, and L. S. Chayes, Phys. Rev. Lett. **96**, 104302 (2006).
[14] *Mathematical Modeling of Collective Behavior in Socio-Economic and Life Sciences*, edited by G. Naldi, L. Pareschi, and G. Toscani (Birkhauser, Boston, 2010), pp. 297–336.
[15] A. A. Chepizhko and V. L. Kulinskii, Physica A **389**, 5347 (2010).
[16] P. Degond, A. Frouvelle, and J.-G. Liu, Seminare Laurent Schwartz EDP Appl. **2012-2013**, 1 (2013).
[17] D. Helbing, Rev. Mod. Phys. **73**, 1067 (2001).
[18] D. Helbing, *et al.*, Environ. Plan. B **28**, 361 (2001).
[19] A. Johansson, D. Helbing, and K. Shukla, Adv. Complex Sys. **10**, 271 (2007).
[20] F. Dietrich and G. Koster, Phys. Rev. E **89**, 062801 (2014).
[21] D. Helbing and P. Molnár, Phys. Rev. E **51**, 4282 (1995).
[22] D. Helbing, P. Molnar, and F. Schweitzer, Evol. Nat. Struct. **9**, 229 (1994).
[23] D. Helbing *et al.*, Pedestrian Evac. Dyn. **21**(2), 21 (2002).
[24] A. Smith, Safety Sci. **47**, 395 (2009).
[25] J. Zhang *et al.*, J. Stat. Mech. (2011) P06004.
[26] S. Bouzat and M. N. Kuperman, Phys. Rev. E **89**, 032806 (2014).
[27] S. Heliövaara, H. Ehtamo, D. Helbing, and T. Korhonen, Phys. Rev. E **87**, 012802 (2013).
[28] D. Helbing, Complex Syst. **6**, 391 (1992).
[29] D. Helbing, Physica A **193**, 241 (1993).
[30] F. Thüroff, C. A. Weber, and E. Frey, Phys. Rev. Lett. **111**, 190601 (2013).
[31] E. Bertim, M. Droz, and G. Gregoiro, J. Phys. A **42**, 445001 (2009).
[32] J. Toner and Y. Tu, Phys. Rev. Lett. **75**, 4326 (1995).
[33] J. Toner, Y. Tu, and S. Ramaswamy, Ann. Phys. (NY) **318**, 170 (2005).
[34] M. C. Marchetti *et al.*, Rev. Mod. Phys. **85**, 1143 (2013).
[35] N. V. Brilliantov and T. Pöschel, *Kinetic Theory of Granular Gases* (Oxford University Press, Oxford, 2010).
[36] B. Kunwar, F. Simini, and A. Johansson, Phys. Rev. E **93**, 032311 (2016).
[37] D. Helbing, I. Farkas, and T. Vicsek, Nature (London) **407**, 487 (2000).
[38] C. A. Weber, F. Thüroff, and E. Frey, New J. Phys. **15**, 045014 (2015).
[39] R.-Y. Guo *et al.*, Transport. Res. Part B **46**, 669 (2012).
[40] W. Kemloh *et al.*, Adv. Complex Syst. **15**, 1250029 (2012).

[41] W. J. Yu, R. Chen, L. Y. Dong, and S. Q. Dai, Phys. Rev. E **72**, 026112 (2005).
[42] S. Cao, J. Zhang, D. Salden, J. Ma, C. Shi, and R. Zhang, Phys. Rev. E **94**, 012312 (2016).
[43] X. Zheng, and Y. Cheng, Comput. Math. Appl. **62**, 4627 (2011).
[44] M. Campanella *et al.*, Transp. Res. Rec.: J. Transp. Res. Board **2124**, 148 (2009).
[45] R. C. Hidalgo, D. R. Parisi, and I. Zuriguel, Phys. Rev. E **95**, 042319 (2017).
[46] D. Helbing, A. Johansson, J. Mathiesen, M. H. Jensen, and A. Hansen, Phys. Rev. Lett. **97**, 168001 (2006).
[47] A. Garcimartín, J. M. Pastor, L. M. Ferrer, J. J. Ramos, C. Martín-Gómez, and I. Zuriguel, Phys. Rev. E **91**, 022808 (2015).
[48] R. Arévalo, I. Zuriguel, D. Maza, and A. Garcimartín, Phys. Rev. E **89**, 042205 (2014).
[49] Tobias Kretz *et al.*, J. Stat. Mech. (2006) P10014.
[50] C. Lozano, A. Janda, A. Garcimartín, D. Maza, and I. Zuriguel, Phys. Rev. E **86**, 031306 (2012).
[51] I. Zuriguel, J. Olivares, J. M. Pastor, C. Martín-Gómez, L. M. Ferrer, J. J. Ramos, and A. Garcimartín, Phys. Rev. E **94**, 032302 (2016).
[52] G. A. Frank and C. O. Dorso, Physica A **390**, 2135 (2011).
[53] J. Starke *et al.*, in *17th International IEEE Conference on Intelligent Transportation Systems (ITSC), Qinqdao, China, 2014* (IEEE, Piscataway, NJ, 2014), pp. 560–565.
[54] D. Helbing, I. J. Farkas, and T. Vicsek, Phys. Rev. Lett. **84**, 1240 (2000).
[55] D. Chaudhuri, Phys. Rev. E **90**, 022131 (2014).
[56] P. Romanczuk, and L. Schimansky-Geier, Phys. Rev. Lett. **106**, 230601 (2011).
[57] H. E. Stanley, Nature (London) **404**, 718 (2000).
[58] M. E. Cates, J. P. Wittmer, J.-P. Bouchaud, and P. Claudin, Phys. Rev. Lett **81**, 1841 (1998).
[59] A. Santos, S. B. Yuste, M. L. de Haro, and Vitaliy Ogarko, Phys. Rev. E **96**, 062603 (2017).
[60] Y. Fily and M. C. Marchetti, Phys. Rev. Lett. **108**, 235702 (2012).
[61] H. Chaté, F. Ginelli, G. Grégoire, and F. Raynaud, Phys. Rev. E **77**, 046113 (2008).
[62] M. Isobe, D. Helbing, and T. Nagatani, Phys. Rev. E **69**, 066132 (2004).
[63] D. Helbing, A. Johansson, and H. Z. Al-Abideen, Phys. Rev. E **75**, 046109 (2007).
[64] Y. Fukuzaki *et al.*, A pedestrian flow analysis system using Wi-Fi packet sensors to a real environment, in *Proceedings of the 2014 ACM International Joint Conference on Pervasive and Ubiquitous Computing: Adjunct Publication, Seattle, Washington*, (ACM, New York, 2014), pp. 721–730.
[65] C. Mankoc, A. Garcimartín, I. Zuriguel, D. Maza, and L. A. Pugnaloni, Phys. Rev. E **80**, 011309 (2009).
[66] V. Lobaskin and M. Romenskyy, Phys. Rev. E **87**, 052135 (2013).
[67] I. Rhee *et al.*, IEEE/ACM Trans. Netw. **19**, 630 (2011).
[68] F. Zanlungo, D. Brscic, and T. Kanda, Phys. Rev. E **91**, 062810 (2015).
[69] T. Shimada, D. Kadau, T. Shinbrot, and H. J. Herrmann, Phys. Rev. E **80**, 020301(R) (2009).
[70] R.-Y. Guo and H.-J. Huang, J. Stat. Mech. (2011) P04018.
[71] L. Peng *et al.*, Phys. Rev. Lett. **79**, 026113 (2009).
[72] L. E. Aik, Int. J. Phys. Sci. **7**, 180 (2012).
[73] L. E. Aik, Int. J. Phys. Sci. **6**, 3218 (2011).
[74] L. Zhang, J. Wang, and S. Qiongyu, J. Sys. Sci. Complex **27**, 430 (2014).
[75] A. Garcimartin *et al.*, Sci. Rep. **7**, 10792 (2017).
[76] O. Corradi *et al.*, SIAM J. Appl. Dyn. Sys. **11**, 1007 (2012).
[77] F. Radjai and S. Roux, Phys. Rev. Lett. **89**, 064302 (2002).
[78] R. Großmann, P. Romanczuk, M. Bär, and L. Schimansky-Geier, Phys. Rev. Lett. **113**, 258104 (2014).
[79] W. Yu and A. Johansson, Phys. Rev. E **76**, 046105 (2007).